DOI: 10.31401/WS.2020.proc.16

A Comparison of the Neutron Dose Measurements Completed by the Bulgarian and Russian Instruments Outside the Zvezda Module of the ISS

Dachev[1] T., Semkova[1] J., Tomov[1] B., Matviichuk[1] Y., Dimitrov[1] P., Koleva[1] R., Jordanova[1] M., Bankov[1] N., Litvak[2] M., Mitrofanov[2] I., Golovin[2] D., Kozyrev[2] A., Malakhov[2] A., Mokrousov[2] M., Sanin[2] A., Tretyakov[2] V., Fedosov[2] F., Ploc[3] O., Shurshakov[4] V., Benghin[4] V.

[1]Space Research and Technology Institute, Bulgarian Academy of Sciences, Sofia, Bulgaria
E-mail: tdachev@bas.bg
[2]Space Research Institute, Russian Academy of Sciences, Moscow, Russia
[3]Nuclear Physics Institute, Czech Academy of Sciences, Prague, Czech Republic
[4]State Research Center Institute of Biomedical Problems, Russian Academy of Science, Moscow, Russia

Abstract

The aim of this article is to compare the neutron dose measurements completed by the Bulgarian and Russian instruments outside the Zvezda module of the International Space Station (ISS). The data from two instruments are used. The Bulgarian Liulin type spectrometer R3DR [Dachev et al., 2015] and the Russian BTN device [Litvak et al. 2017]. Both instruments were mounted outside the Zvezda module of the ISS.

The first part of the paper describes both instruments and illustrates that they are situated at a 4-5 meters apart from each other. A detailed description of the procedure for the evaluation of the ambient dose equivalent ($H^*(10)$) is presented.

The assessment of the equivalent dose rates of neutron radiation, measured by BTN and R3DR instruments, reveals that R3DR and BTN values are comparable in both equatorial and South Atlantic Anomaly (SAA) regions, while the R3DR values are higher that the BTN values in the high latitude regions.

Introduction

Neutrons at the height of the board the International Space Station (ISS) are produced in three physical processes [Tret'yakov et al., 2010]. First, energetic protons and ions from the galactic cosmic rays and from the radiation belts of the Earth's magnetosphere generate neutrons with energies of about 10-20 MeV due to the nuclear reactions in the upper atmosphere of the Earth. The produced secondary neutrons are slowed in the atmosphere matter. Part of them are absorbed in the nuclear reactions of capture to form new nuclei. Another part is decayed, but a substantial fraction leaves the atmosphere [Nymmik, 1993], forming in the near-terrestrial space the so-called neutron albedo of the Earth.

Second, around the ISS the proper induced neutron emission is produced due to the interactions of the energetic charged particles of the magnetosphere with the matter of the station itself [Sevast'yanov et al., 1997]. These local neutrons fluxes are present around the station and they are variable along the station orbit due to irregularity of the flux of charged particles.

The third cause of the existence of neutrons in the near-terrestrial space is the solar activity. It is well known that during some powerful solar energetic particles (SEPs) fluxes of high-energy neutrons are generated [Share et al., 2007], [Xiao et al. 2016] reports a total of 12 solar events in which neutrons even reached the Earth ground between 1982 and 2015.

Instrumentation

BTN instruments description

The BTN-MD detection block (Fig. 1) is a spectrometer with four individual neutron detectors. BTN-MD is a spare flight unit of the HEND experiment, installed onboard NASA spacecraft Mars Odyssey, intended for the exploration and cartography of neutron radiation of Mars surface in different energy ranges [Mitrofanov et al., 2002]. After several years of successful operation of HEND, it was decided to use a spare flight unit for the near Earth measurements onboard the ISS [Tret'yakov et al., 2010]. The Russian Zvezda module was chosen for this. Some preparations were made, such as development of the BTN-ME inner control block, the Block-MF (a system for providing temperature conditions) and a special mounting pylon for the BTN-MD outside the station [Tret'yakov et al., 2010].

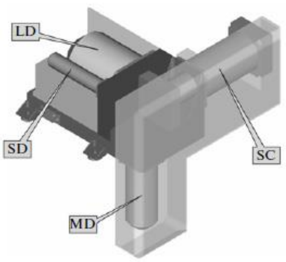

Fig. 1. Structure chart of the BTN-MD unit.

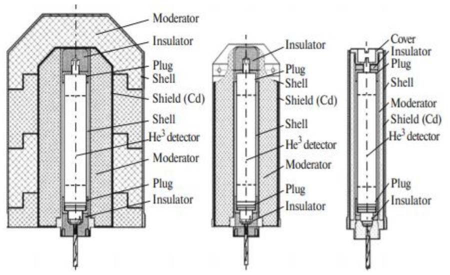

Fig. 2 Design features of BTN-MD instrument

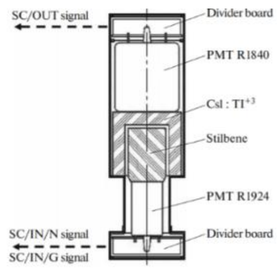

Fig. 3. Scintillation block configuration.

Three detectors (SD, MD, LD (pls. see Fig. 2.) are based on helium-filled (^{3}He) proportional neutron counters, covered in cadmium shields and polyethylene spheres of different thickness [Litvak et al. 2017]. The proportional ^{3}He counters are detectors of epithermal neutrons. In this case, having given a good account (also as a part of the HEND experiment flight unit), the LND2517 industrial counters (LND Inc. Company, United States) were used, filled with ^{3}He and a small addition of CO_2 under an atmosphere pressure of 6. The registration concept in the proportional counter is based on the capture of a thermal or epithermal neutron in a reaction of that type as follows:

$$n + {}^3He \rightarrow {}^3H + p + 764\ keV \quad (1)$$

The total energy output in that reaction is distributed between the proton and the triton in the ratio of 191 keV (triton) and 573 keV (proton) in inverse proportion to their masses.
The counter itself is a metallic cylinder (cylinder jacket serves as a cathode) with a thin (thickness about the fraction of a millimeter) tungsten wire along the cylinder axis, which serves as the anode. A current of about 1 kV is applied between the cathode and the anode. This allows the counter to work in the so-called proportional mode, when the applied current is high enough for the primary electrons formed during the ionization of gas molecules by a nuclear reaction of $n + {}^3He \rightarrow {}^3H + p$ in order to perform a secondary ionization with the generation of a large number of ion pairs. The collected charge on the electrodes of the counter and the corresponding current impulse is proportional to the full energy output in the volume of the counter. The digitalization of the signal received, during one neutron registration act, allows the amplitude spectrum to be obtained.

The fourth detector (SC (pls. see Fig. 3.) is intended to register only high-energy neutrons in the energy range of 350 keV to 15 MeV. It was manufactured from a stilbene crystal (C14H12) and covered with the anticoincidence shield from the crystal.

Figure 4 shows the sensitivity functions of all detectors in the BTN-MD instrument. It is clearly seen that, due to various thicknesses of the moderators, in the proportional counters, we managed to succeed in registering neutrons in a wide range of energies of from 0.4 eV up to 15 MeV.

R3DR instruments description

The EXPOSE-R missions on the ISS was performed by the European Space Agency (ESA) for astrobiological studies under space conditions as provided in low-Earth orbit outside the ISS. [Rabbow et al., 2015]. The radiation fields encountered in this environment is of pivotal interest to astrobiology [Ferrari and Szuszkiewicz, 2009]. To provide information about the diurnal variation of this radiation, the EXPOSE-R platform accommodated the Radiation Risk Radiometer-Dosimeter (R3D) for the Russian segment (R) R3DR (Fig. 5). It is a low mass and small-dimension automatic device measuring solar radiation in four channels and cosmic ionizing radiation in 256 channels during the EXPOSE-R mission in 2008-2009. R3DR instrument was developed and build in cooperation by Bulgarian and German scientists after a successful participation in the ESA announcements of opportunity in 1996, 2001 and 2003 [Dachev et al., 2015 and 2017].

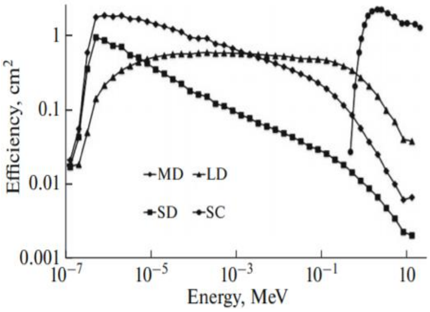

Fig. 4. Sensitivity functions for all BTN-MD instrument detectors.

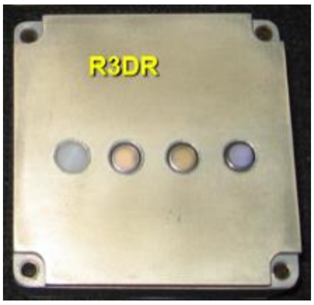

Fig. 5. R3DR instrument.

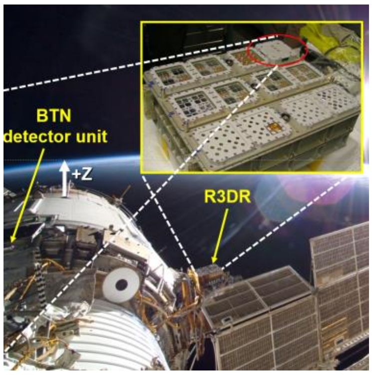

Fig. 6 Position of the BTN detector unit and R3DR instrument outside ISS Zvezda module.

The R3DR instrument is single detector Liulin type spectrometer. Its block diagram and dose calculation procedure are described in the paper by Dachev et al., named "Registration of neutrons with a single detector Liulin type spectrometer" in this issue.

Recently, Dachev et al., (2017) published a comprehensive description of the R3DR2 instrument and its radiation sources selection procedures. Therefore, we will skip those details, as R3DR unit is identical to the R3DR2.

Fig. 6 shows the mounting position of the EXPOSE-R platform with the mounted inside R3DR instrument and the BTN detector at the left side of the Russian Zvezda module of the ISS. The BTN detector unit is seen in the zenith area of the module. Both units, BTN detector and R3DR instrument, are at a distance of about 4-5 meters.

Energy deposition spectra variations by source and location

Fig. 3 of the paper by Dachev et al., named "Registration of neutrons with a single detector Liulin type spectrometer" in this issue presents the shapes of the galactic cosmic ray (GCR) spectra only.

Fig. 7 here illustrates the shapes of all three-radiation sources for the period May 1, 2010-July 11, 2010. There are two spectra for the GCR, one for the high latitudes (HL) and another for the equatorial (Eq) latitudes. Two more spectra are included – one for the outer radiation belt (ORB) and one for the inner radiation belt (IRB).

Fig. 8 visualizes the geographic locations of the different areas and sources, mentioned in Fig. 7. The isolines of the L-shell values from 1 to 5 for the 2005 epoch [McIlwain, 1961; Heynderickx et al., 1996] at the altitude of the ISS are presented with pink dashed lines in Fig. 8. The equatorial GCR region is seen with red ellipse where the effective cutoff rigidity - R_c values are greater than 15.4 GV. This region is in the middle of the L, equal to one isoline.

The south and north high latitude (HL) regions are plotted with blue areas. They are characterized by R_c less than 0.85 GV in north and 0.62 GV in the south hemispheres respectively. These definitions of the GCR source locations was used by Litvak et al., (2017). Here we apply the same definitions to make the comparisons presented in Table 1. (R_c values were calculated using the Shea et al., (1985) relations between L-shell parameter and R_c values.)

The IRB region is seen with light green area, where the total Earth magnetic field strength is less than 0.24 Gauss.

The light brown points show the positions where the ORB particles were observed in 2015. The maximum at about 20° East longitude with L=2.5 gives the ORB position during the magnetic storms [Dachev, 2018 see Fig. 2 therein].

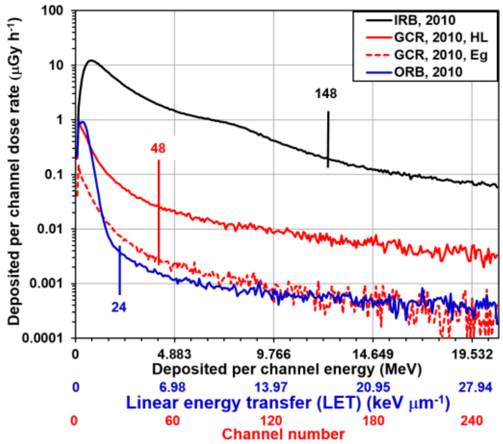

Fig. 7. A comparison of the spectra shapes by different radiation sources.

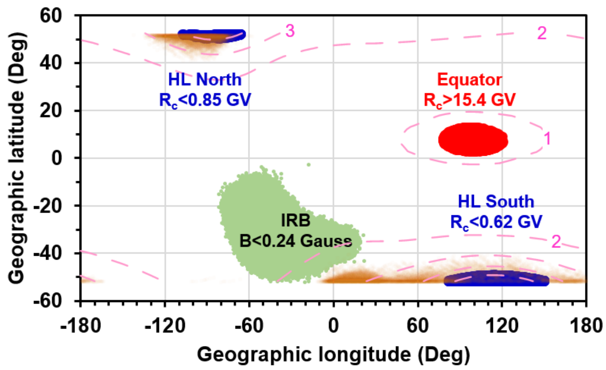

Fig. 8. The global distribution of places in Fig. 7.

In Fig., 7 the deposited per channel dose rates in μGy h^{-1} are plotted against the deposited per channel energies in MeV. For a better understanding of the Fig. 7, two additional horizontal axes are added below the main horizontal axes. They are the linear energy transfer in keV μm^{-1} and the channel number.

Fig. 7 clarifies the selection procedure of the high and low LET parts of the spectra. The ORB and GCR spectra curves shapes are similar, showing a part with a high slope in the low LET energy deposition region and a smaller slope part in the high LET. We consider that the end of the low LET part of the spectra is at the point of the slope changes. There the low LET part finishes and the high LET part of the spectrum begins. From Fig. 7 it is seen that for the GCR source, the selection point is at channel 48, while for the ORB source it is at channel 24.

Fig. 7 depicts that the GCR low LET source spectra part shows a maximum up to 0.1 μGy h^{-1}, which has to be populated by high-energy protons from a galactic origin. Above channel number 48, the spectra continues with a small slope part that contains mainly secondary neutrons protons penetrating trough the side walls of the detector and neglectable amount of He^+ ions.

There are two GCR spectra in Fig. 7. The higher dose rate spectrum presents the averaged dose rates in the high latitude (HL) regions, while small dose rate spectrum presents the equatorial region (Eq). The explanation is that the high latitude spectrum contains larger amount of primary GCR particles, being in smaller vertical cutoff rigidity [Smart & Shea, 2005].

The IRB spectra in Fig. 7 is obtained inside of the inner radiation belt at a total magnetic field strength B less than 0.24 Gauss. It is populated mainly by protons in the energy range 10–200 MeV [Nealy et al., 2007]. The two main peculiarities seen in the shape of this spectrum are:

(a) The maximum in the deposited dose is close to 0.9 MeV deposited energy. It is generated by the SAA mean energy protons of about 40 MeV [Dachev et al., 2017a];

(b) There is a knee at about 9.1 MeV deposited energy.

Usually the change of the slope of the IRB spectrum appears close to 6 MeV deposited energy at channel 78. This corresponds to the stopping energy of the normally falling protons to the detector with 0.3 mm thickness [Dachev, 2009]. The exact value for 0.3 mm silicon is 6.2 MeV as seen in the tables provided by Berger et al. [2020] at http://physics.nist.gov/PhysRefData/Star/Text/contents.html. Similar result was obtained during the calibrations of Liulin 4 type instrument with 7.8 MeV incident energy protons, falling normally to the detector (Fig. 4 of Dachev et al., 2017a). 6.2 MeV deposited energy is registered in the channel 78. This means that all other channels up to 256 of the spectrometer are populated by long path length low LET protons or by heavier ions. In the specific case, the R3DR spectrum is moved to the right and is registered in channel 93. The reason is the place where R3DR spectrometer is located (Fig. 6). The latter is mounted very close to the body of Zvezda module, which partially shielded the SAA protons, drifting almost horizontally from West to East. In order to keep the same requirements for the selection procedure of the high and low LET parts of the spectrum, we decided to choose as a point of change of the slope of the IRB spectrum to channel 148.

The ORB spectrum (Fig. 7) shows huge maximum up to 1.5 μGy h^{-1}in the channel numbers 0 to 24. This part of the spectrum is populated by relativistic electrons, trapped in the ORB. The spectrum slope, registered between channels 24 and 256, is very similar to the GCR spectrum slope. This is reasonable because the relativistic ORB electrons are observed at high latitude regions (please look Fig. 8), where the GCR particles are the main permanently detected source.

Evaluation of the ambient dose equivalent (*H(10)) with SDLTS**

Bartlett et al., [2006] wrote, "Secondary neutrons generated from the primary galactic cosmic radiation and trapped particles can be a major contributor to dose equivalent and effective dose on a spacecraft and ISS. The amount of shielding of the primary radiation manage the exact proportion, which lie in the range of 10–60%."

Benton et al., [2001] wrote, "Dose equivalent rate measurements of neutrons with energies >1 MeV ranged from 4.5 μSv d^{-1} on the low altitude STS-3 mission to 172 μSv d^{-1} on the ~6 year LDEF mission. Thermal neutrons (<0.3 eV) were observed to make a negligible contribution to neutron dose equivalent in all cases. The major fraction of neutron dose equivalent was found to be from neutrons >1MeV and, on LDEF, neutrons >1MeV are responsible for over 98% of the total neutron dose equivalent. Estimates of the neutron contribution to the total dose equivalent are somewhat lower than model estimates, ranging from 5.7% at a location under low shielding on LDEF to 18.4% on the highly inclined (82.3°) Biocosmos-2044 mission". https://doi.org/10.1016/S1350-4487(01)00047-6

Our assumption is that the R3DR instrument has the sensitivity to detect neutrons is based on the:

(1) Calibration results, presented in the paper Dachev et al., "Registration of neutrons with a single detector Liulin type spectrometer" in this issue.

(2) The simulations by the computer codes FLUCA, GEANT4 and PHITS, performed by Luszik-Bhadra et al. [2010] to investigate the "Response calculations for silicon-based direct-reading dosimeters for use at the International Space Station". This paper has a section, which uses the LULIN type geometry. It estimates the expected dose equivalent. The highest effective dose equivalent is obtained from protons (178 μSv d^{-1}), followed by Fe ions (44 μSv d^{-1}), neutrons (23 μSv d^{-1}) and He ions (13 μSv d^{-1}). The mean dose equivalent as calculated for the DOS-2005 and the LIULIN devices agrees with the calculated values of effective dose equivalent better than a factor of two.

(3) The calibrations performed in CERN by Zhang et al., [2011] to investigate the fast neutron induced nuclear counter effect in Hamamatsu S2744-08 silicon PIN diodes that are the same as the diodes used by us in the R3DR instrument.

According to [Benton et al., 2001] and the results shown in Fig. 4 of [Dachev et al., Registration of neutrons with …, this issue], we expect that we may detect by the single detector Liulin type spectrometers (SDLTS) neutrons with energies between 1 and 50 MeV.

Historically, two attempts for the calculation of the SDLTS ambient dose equivalent (*H**(10)) at spacecraft altitudes were developed. Both are based on the similarity of the neutron spectra at aircraft and spacecraft altitudes [Bartlett et al., 2006], http://wrmiss.org/workshops/tenth/pdf/ex01_bartlett.pdf (pls. see slide No 11 therein).

We calculate the ambient dose equivalents from the measurements using the quality factor (Q) as defined in the [ICRP Report No. 60].

In the first attempt [Spurny et al., 2006, 2007, 2009] *H**(10) is calculated from the deposited energy spectra, supposing that events with deposited energy less than 1 MeV correspond to low LET radiation and events with deposited energy higher than 1 MeV correspond to the sum of the neutron and heavier charged particles (HECP) of the GCR. The data were treated in the following way:

a) For the low LET component *D*(Si)→*D*(tissue)→ *H**(10);

b) For the neutron contribution in the region of *E*dep>1 MeV. This is the same procedure as on board aircraft [Spurny and Dachev, 2002] that was adopted, considering that the neutron spectra are in both cases similar [Bartlett et al., 2006, pls. see slide No 9 therein]. The supposed average quality factor for this component of galactic cosmic radiation is equal to about 5;

c) For the HECP *H**(10) is obtained as: *D*(Si)→*D*(tissue); 5×*D*(tissue)= *H**(10); i.e., supposing that the average quality factor for this component of the galactic cosmic radiation is equal to about 5;

d) For the flights inside the IRB, is supposed that all events are due to protons with average QF~1.3, calculated from the energy deposition spectra in Si detector of MDU-Liulin. Finally, the following equations were used:

$$H^*(10) = Q_1 * D_{Low\ LET} + Q_2 * D_{High\ LET} \qquad (3)$$

$$H_{\mathrm{GCR}}{}^*(10) = 1 * \sum_1^{14}(\mathrm{Ei} * \mathrm{Ai})/\mathrm{MD} + 5 * \sum_{15}^{256}(\mathrm{Ei} * \mathrm{Ai})/\mathrm{MD} \qquad (4)$$

$$H_{IRB}{}^*(10) = 1.3 * \sum_1^{14}(\mathrm{Ei} * \mathrm{Ai})/\mathrm{MD} + 1.3 * \sum_{15}^{256}(Ei * Ai)/MD \qquad (5)$$

In the above preliminary equations, the deposited energy in channel number 14 is equal to 1 MeV deposited energy. Equation number (4) was used for a calculation of the ambient dose equivalent (*H**(10)) at aircraft altitudes.

The equations above were used for a comparison of the calculated *H**(10), obtained with Liulin-E094 in 2001 and R3DE instruments in 2008 with NASA TEPC at the ISS (https://srag.jsc.nasa.gov/SpaceRadiation/How/How.cfm). The obtained satisfactory results were published in 2010 [Dachev et al., 2010, http://wrmiss.org/workshops/fifteenth/Dachev.pdf].

Fig. 9 shows in details the comparison of absorbed and equivalent doses obtained by R3DE instrument and NASA TEPC in 2008.

The second attempt for the calculation of the SDLTS and particularly of the R3DR ambient dose equivalents (*H**(10) from neutrons is described in the next paragraphs of this paper, i.e.:

It is assumed that the end of the low LET part of the deposited energy spectra for the different sources of radiation as GCR, IRB and ORB is at different channels numbers, i.e. 48 for the GCR, 148 channel for the IRB and 24 for the ORB. This is well illustrated in Fig. 7 as well as on Fig. 5d and Fig. 6a in the paper by Dachev et al. "Registration of neutrons with a single detector Liulin type spectrometer" in this issue.

The first attempt for the calculation of the ambient dose equivalents (*H**(10) assumes that the deposited energy in channel number 14 (equal to 1 MeV deposited energy) is the last channel of the low LET part of the deposited energy. It is fixed for all radiation sources.

As our goal is the comparison of the neutron dose equivalents, measured with the BTN instrument, only the high LET part of the following equations are used.

$$H_{GCR}{}^*(10) = 3.16 * \sum_{48}^{256}(\mathrm{Ei} * \mathrm{Ai})/\mathrm{MD} \qquad (6)$$

$$H_{IRB\ and\ SEP}{}^*(10) = 1.7 * \sum_{148}^{256}(\mathrm{Ei} * \mathrm{Ai})/\mathrm{MD} \qquad (7)$$

$H_{ORB}{}^*(10) = 1 * \sum_{24}^{256}(\mathrm{Ei} * \mathrm{Ai})/\mathrm{MD}$ (8)

The conversion quality factors for GCR (Q=3.16) and IRB (Q=1.7) sources in the equations (6) and (7) was obtained by averaging of 923,114 measurements in the CGR source and 60,973 in the "Trapped" source performed by the NASA TEPC in the period from Mach 1, 2008 till March 31, 2010 [https://www.nasa.gov/mission_pages/station/science/experiments/TEPC.html]. The TEPC data were provided by [Zapp, 2013] and by the Coordinated Data Analysis Web' at the Goddard Space Flight Center [http://cdaweb.gsfc.nasa.gov/].

Luszik-Bhadra et al. [2010] in Fig 2 therein limited the list of the heavier ions to Helium and Iron. Iron ions are out of the range of the SDLTS [Uchihori et al. 2002]. The amount of He^+ ions in the spectral fluence rate in the cited above Fig. 2 of Luszik-Bhadra et al. [2010] in the energy range 10-100 MeV are two orders of magnitude below that of the neutrons fluence rate

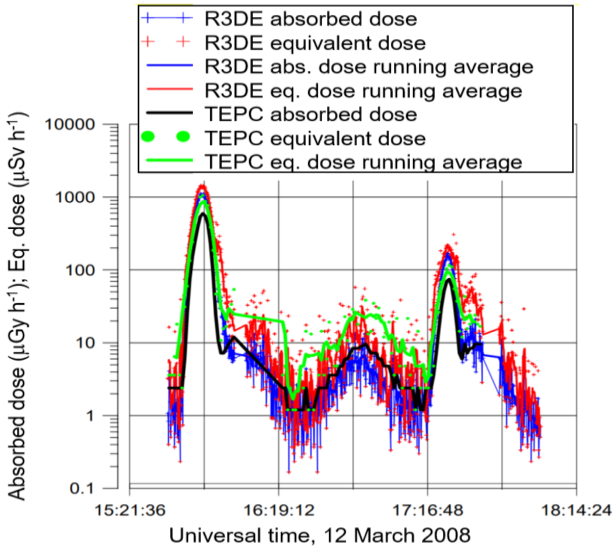

Fig. 9. A comparison of absorbed and equivalent doses obtained by R3DE instrument and NASA TEPC.

outside the ISS. That is why; we decided to neglect this very low fluence rate of He^+ ions and to consider that the completely high LET parts of the GCR, IRB and ORB spectra are populated only by neutrons.

Comparisons of the averaged neutron equivalent dose rates

The equations 6-8, described in the previous section, were used to calculate the equivalent dose rates measured by R3DR instrument in the period May 1, 2010- July 11, 2010.

Table 1 presents the results from the comparison of the equivalent dose measurements at various segments of the orbit. Three experiments are listed: BBND inside the ISS [Koga et al., 2011], BTN outside the ISS [Tret'yakov et al., 2010], [Litvak et al. 2017] and R3DR outside the ISS [Dachev et al., 2015].

Table 1.

Experiment, Dates of measurements, Solar activity level	**Measurement condit., Detectors, Range of measurements**	**Estimation of the average neutron equivalent dose rate accumulation at various segments of the orbit, µSv h⁻¹**			
		GCR		**IRB (SAA)**	**ORB**
		Equator	**High lat. (HL)**		
BBND [Koshishi et al., 2007], Mar 23, 2001–Nov 15, 2001, Max. of 23rd cycle	Inside the ISS, 6 sensors ^{3}He and one scintillation detector, 0.03 eV–15.0 MeV	0.3-1	2-6	10-100	

BTN, [Tret'yakov et al., 2010], Feb 26–present time, A half of the solar activity cycle	Outside the ISS 3 sensors ^{3}He and one scintillation detector, 0.4 eV–10.0 MeV	0.2	0.8	5	
BTN, [Litvak et al., 2017], Feb 26–present time, A half of the solar activity cycle	Outside the ISS 3 sensors ^{3}He and one scintillation detector, 0.4 eV–10.0 MeV	0.1-0.4	1-5	>50	
R3DR, [Dachev et al., 2015] May 1, 2010- July 11, 2010 Minimum of the solar activity cycle	Outside the ISS, One PIN diode detector, 1-50 MeV	0.43	6.3	21	4

Table 1 reveals that the both the BBND and R3DR average equivalent dose rates are similar in the high latitudes and the SAA region. Close to the equator, the BBND dose values [Koga et al., 2011] are about 8 times higher than the R3DR values.

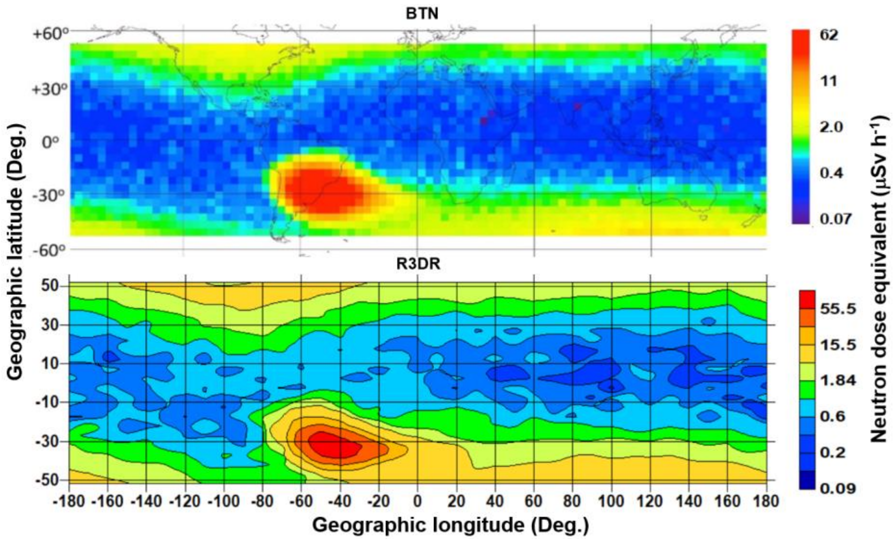

Fig. 10. Equivalent dose rate of neutron radiation measured by BTN and R3DR spectrometer.

The comparison of the equivalent dose rate values obtained with R3DR instrument and BTN shows the following:

a) The BTN values close to the equator are comparable with the R3DR values;

b). The probable reason is that the energy range of the measured neutrons of the R3DR instrument is from 1 to 50 MeV, while the BTN range is up to 16 MeV.

c) In the SAA region the average equivalent dose rates, registered with BTN and R3DR are comparable.

d) Only R3DR has measured the average equivalent dose rates in the ORB region.

Fig. 10 illustrates the comparison of the global distribution of the equivalent dose rate of neutron radiation measured by BTN and R3DR spectrometer. At first glance, both distributions are quite similar. The distributions demonstrate the dependence from the Earth magnetic field and follow the global distribution of the L-values.

Fig. 10 confirms the results listed in Table 1, i.e.: R3DR values are higher that the BTN values in the high latitudes; R3DR and BTN values are comparable in both equatorial and SAA regions.

Conclusions

This paper compares the neutron dose measurements, completed by the Bulgarian R3DR spectrometer and Russian BTN instrument. They both were mounted outside the Zvezda module of the International Space Station.

The assessment of the equivalent dose rates of neutron radiation, measured by BTN and R3DR instruments, reveals that R3DR and BTN values are comparable in both equatorial and South Atlantic Anomaly (SAA) regions, while the R3DR values are higher that the BTN values in the high latitude regions.

Acknowledgements
This work is supported by: Agreement between RAS and BAS on "Fundamental space research", Contract No. 4000117692/16/NL/NDe Funded by the Government of Bulgaria through an ESA Contract under the PECS (Plan for European Cooperating States), Contract with National Science Fund –Bulgaria on Project N 129 FOR BILATERAL PROJECTS – BULGARIA – RUSSIA 2018 -2019. In IKI-RAS the work is supported by the Russian Science Foundation under grant 19-52-18009. NPI work was funded by the European Structural and Investment Funds under the Operational Program Research, Development and Education (project CRREAT CZ.02.1.01/0.0/0.0/15_003/0000481).

Most of the data used in this paper are part of the "Unified web-based database with Liulin-type instruments", which are available online, free of charge at the following URL: http://esa-pro.space.bas.bg/database. The database was created under the ESA contract mentioned above.

References

Bartlett D.T. and Goldhagen P. (2005), private communication of Prof. Spurny.

Benton, E. R., & Benton, E. V. (2001), Space radiation dosimetry in low-Earth orbit and beyond. Nuclear Instruments and Methods in Physics Research B, 184(1–2), 255–294.

Dachev, Ts.P., (2009), Characterization of near Earth radiation environment by Liulin type instruments, Adv. Space Res., 44, 1441-1449. http://dx.doi.org/10.1016/j.asr.2009.08.007

Dachev, T.P., J.V. Semkova, B.T. Tomov, Yu.N. Matviichuk, Pl.G. S. Maltchev, R. Koleva, Pl., Dimitrov, N.G. Bankov, V.V., Shurshakov, V.V., Benghin, E.N., Yarmanova, O.A. Ivanova, D.-P. Häder, M.T. Schuster, G. Reitz, G. Horneck, Y. Uchihori, H. Kitamura, O. Ploc, J. Kubancak, I. Nikolaev, (2015), Overview of the Liulin type instruments for space radiation measurement and their scientific results, 92–114. http://dx.doi.org/10.1016/j.lssr.2015.01.005.

Dachev, Ts., G. Horneck, D.-P. Häder, M. Schuster, and M. Lebert, (2015), EXPOSE-R cosmic radiation time profile, Journal of Astrobiology, 14, 17-25. http://dx.doi.org/10.1017/S1473550414000093.

Dachev, T. P., Bankov, N. G., Tomov, B. T., Matviichuk, Y. N., Dimitrov, P. G., Häder, D.-P. & Horneck, G., (2017), Overview of the ISS radiation environment observed during the ESA EXPOSE-R2 mission in 2014–2016. Space Weather, 15, 1475–1489. https://doi.org/10.1002/2016SW001580.

Dachev, T.P., (2018). Relativistic Electron Precipitation Bands in the Outside Radiation Environment of the International Space Station, Journal of Atmospheric and Solar-Terrestrial Physics, 177, 247-256. https://doi.org/10.1016/j.jastp.2017.11.008

Ferrari, F. & Szuszkiewicz, E. (2009). Cosmic rays: a review for astrobiologists. Astrobiology 9, 413–136.

ICRU, 2000. Nuclear Data for Neutron and Proton Radiotherapy and for Radiation Protection, Report 63. ICRU Publication, Bethesda, MD.

Koshiishi, H., Matsumoto, H., Chishiki, A., Goka, T. and Omodaka, T., (2007). Evaluation of the neutron radiation environment inside the International Space Station based on the Bonner Ball Neutron Detector experiment. Radiation measurements, 42(9), 1510-1520.

Litvak, M.L., Mitrofanov, I.G., Nuzhdin, I.O. *et al.*, (2017), Monitoring of the time and spatial distribution of neutron-flux spectral density outside the Russian segment of the *International Space Station* based on data from the BTN-Neutron space experiment. *Cosmic Res* 55, 110–123. https://doi.org/10.1134/S001095251702006X

Luszik-Bhadra, M., Beck, P., Berger, T., Jaksic, A., Latocha, M., Rollet, S., Vuotila, M., Zechner, A. and Reitz, G., 2010. Response calculations for silicon-based direct-reading dosimeters for use at the international space station (ISS). Radiation measurements, 45(10), 1548-1552.

McIlwain, C. E., (1961). Coordinates for mapping the distribution of magnetically trapped particles. Journal of Geophysical Research, 66, 3681–3691. https://doi.org/10.1029/JZ066i011p03681.

Mitrofanov, I.G., Litvak, M.L., Kozyrev, A.S., et al., (2003). Search for water in Martian soil using global neutron mapping by the Russian HEND instrument onboard the US 2001 Mars Odyssey spacecraft, Sol. Syst. Res., vol. 37, 5, 366–377.

Nealy, J.E. et al. (2007). Pre-engineering spaceflight validation of environmental models and the 2005 HZETRN simulation code. Adv. Space Res. 40, 1593–1610. doi: 10.1016/j.asr.2006.12.030.

Nymmik, R.A., (1993). A Model of Particle Fluxes and Energy Spectra of Solar Cosmic Rays, *Kosm. Issled.*, vol. 31, no. 6, pp. 51–59.

Rabbow, E., Rettberg, P., Barczyk, S., Bohmeier, M., Parpart, A., Panitz, C., … Reitz, G. (2015). The astrobiological mission EXPOSE-R on board of the International Space Station. International Journal of Astrobiology, 14, 3–16. https://doi.org/10.1017/S1473550414000202

Shavrin, P.I., Kuzhevskij, B.M., Kuznetsov, S.N., et al., (2002). Measurements of neutron fluxes with energies from thermal to several MeV in near-Earth space: SINP results, Radiat. Meas., 35, 5, 531–538.

Sevast'yanov, V.D., Tarnovskii, G.B., and Lyagushin, V.I., (1997). Measurement of the Neutron Energy Spectrum on the Mir Orbital Station, Kosm. Issled., 35, 2, 216–220. [Cosmic Research, pp. 201–205].

Spurný, F., (2005). Response of a Si-diode-based device to fast neutrons, Radiation Measurements, 39, 219 – 223.

Spurný, F., Ploc O., Dachev, T., (2007). On the Neutron Contribution to the Exposure Level onboard Space Vehicles, Radiation Prot. Dosimetry, 126, 519 – 523. http://rpd.oxfordjournals.org/content/126/1-4/519

Spurný, F., Ploc, O., & Jadrníčková, I., (2009). Spectrometry of linear energy transfer and dosimetry measurements onboard spacecraft and aircrafts. Physics of Particles and Nuclei Letters, 6(1), 70-77.Tret'yakov, V.I., Mitrofanov, I.G., Bobronitskii, Yu.I., et al., (2010). The first stage of the "BTN-Neutron" space experiment onboard the Russian segment of the International Space Station, Cosmic Res., 48, 4, 285–299.

Xiao, X.Y.; Hong, L.; Guan, T.Ch.; Xin, Q.L.; Jian, K.S.; Cheng, M.T., 2016. Detection of solar neutron events and their theoretical approach, New Astronomy, 39, 2

Zapp, N., (2013). SRAG group at NASA GSFC, by ′Coordinated data analysis web′ at Goddard Space Flight Center, http://cdaweb.gsfc.nasa.gov/.

Zhang, L., Mao, R. and Zhu, R.Y., 2011. Fast neutron induced nuclear counter effect in Hamamatsu silicon PIN diodes and APDs. *IEEE Transactions on Nuclear Science*, *58*(3), pp.1249-1256.